ARTICLE   OPEN

Low-temperature dielectric anomaly arising from electronic phase separation at the Mott insulator-metal transition

A. Pustogow [1,2,8 ✉], R. Rösslhuber [1,8], Y. Tan[3,8], E. Uykur[1], A. Böhme[1], M. Wenzel[1], Y. Saito[1,4], A. Löhle[1], R. Hübner [1,5], A. Kawamoto[4], J. A. Schlueter[6,7], V. Dobrosavljević [3 ✉] and M. Dressel [1 ✉]

Coulomb repulsion among conduction electrons in solids hinders their motion and leads to a rise in resistivity. A regime of electronic phase separation is expected at the first-order phase transition between a correlated metal and a paramagnetic Mott insulator, but remains unexplored experimentally as well as theoretically nearby $T = 0$. We approach this issue by assessing the complex permittivity via dielectric spectroscopy, which provides vivid mapping of the Mott transition and deep insight into its microscopic nature. Our experiments utilizing both physical pressure and chemical substitution consistently reveal a strong enhancement of the quasi-static dielectric constant ε_1 when correlations are tuned through the critical value. All experimental trends are captured by dynamical mean-field theory of the single-band Hubbard model supplemented by percolation theory. Our findings suggest a similar 'dielectric catastrophe' in many other correlated materials and explain previous observations that were assigned to multiferroicity or ferroelectricity.

INTRODUCTION

Insulator-metal transitions (IMTs) remain one of the unresolved science problems of condensed-matter physics, which are rather general and of fundamental importance. Especially intriguing are those IMTs not associated with static symmetry changes, where paradigms for conventional phase transitions provide little guidance. Early examples of such behavior are found in certain disorder-driven IMTs[1]. In recent years, IMTs with no symmetry breaking were also identified around the Mott transition[2-5], which bears close connection to exotic states of strongly correlated electron matter, such as unconventional superconductivity and quantum spin liquids (QSLs). From a theoretical point of view, the single-band Hubbard model is well understood[6,7], and is found to be in excellent agreement with experiments[5,8-10]. While commonly concealed by antiferromagnetism, recent development in the field of organic QSLs enabled investigation of the low-temperature Mott IMT in absence of magnetic order[11-14], revealing finite-frequency precursors of the metal already on the insulating side[15].

At half filling, the Mott insulator and the correlated metal converge at the critical endpoint T_{crit} (Fig. 1). The former is bounded by a quantum-critical region along the quantum Widom line (QWL)[5,15-18]. On the metallic side, resistivity maxima at the Brinkman-Rice temperature T_{BR} signal the thermal destruction of resilient quasiparticles[19,20] and the crossover to semiconducting transport. Below T_{crit}, the IMT is of first order and comprises an insulator-metal coexistence regime[6,16,17]. Figure 1 displays the phase diagram of genuine Mott systems at half filling without magnetic order[15], as realized in triangular-lattice organic compounds subject to strong geometrical frustration[5,11-14,21]. Note, many oxides are charge-transfer insulators[22] and involve a pronounced coupling of the IMT to the lattice[10,23], whereas the

molecular materials studied here are ideal model systems to elucidate single-band Mott insulators without significant structural modifications at the transition to the metallic state. It is currently debated whether the electrodynamics of the genuine Mott IMT is dominated by closing of the Mott gap or by spatial inhomogeneity, fueled by recent low-temperature transport studies[14].

Although the high-quality crystals we investigate typically feature uniform insulating and metallic phases, the situation is more subtle within the IMT phase-coexistence region at $T < T_{crit}$. Similarly to most other systems close to first-order phase transitions, here one generally expects spatial segregation into domains of the coexisting phases, and the associated metastability and hysteresis phenomena. Seminal transport and susceptibility experiments indeed found a pronounced hysteresis in the Mott systems V_2O_3 and κ-(BEDT-TTF)$_2$Cu[N(CN)$_2$]Cl featuring magnetically-ordered ground states[8,9,24]. Unfortunately, analogue measurements with continuous pressure tuning are not feasible on QSL compounds, such as κ-(BEDT-TTF)$_2$Cu$_2$(CN)$_3$, due to the low temperatures ($T < 20$ K) and high pressures ($p > 1$ kbar) required to cross the first-order IMT. Alternative methods are, therefore, required in these systems in order to reveal and map-out regimes where such inhomogeneous electronic states arise. While different microscopic mechanisms can, in principle, contribute to stabilizing such inhomogeneous phase separation (see discussion below), in electronic systems it proves to dramatically modify the electrodynamic response leading to robust percolation phenomena that depend only weakly on the system-dependent details. This observation, as we shall demonstrate below, allows us to clearly recognize and understand the regime dominated by phase coexistence, resolving much of the controversy associated with the nature of the Mott point in QSL compounds.

[1]Physikalisches Institut, Universität Stuttgart, 70569 Stuttgart, Germany. [2]Department of Physics and Astronomy, UCLA, Los Angeles, CA 90095, USA. [3]Department of Physics and National High Magnetic Field Laboratory, Florida State University, Tallahassee, Florida 32306, USA. [4]Department of Physics, Hokkaido University, Sapporo 060-0810, Japan. [5]Inst. für Klinische Radiologie und Nuklearmedizin, Universität Heidelberg, Mannheim, Germany. [6]Material Science Division, Argonne National Laboratory, Argonne, IL 60439-4831, USA. [7]Division of Materials Research, National Science Foundation, Alexandria, VA 22314, USA. [8]These authors contributed equally. A. Pustogow, R. Rösslhuber, Y. Tan. ✉email: andrej.pustogow@pi1.physik.uni-stuttgart.de; vlad@magnet.fsu.edu; dressel@pi1.physik.uni-stuttgart.de
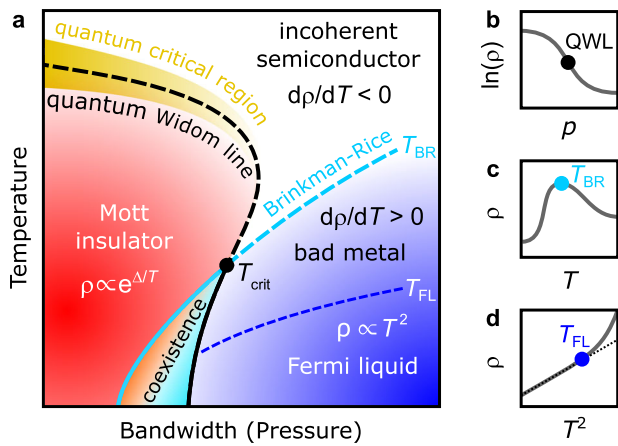
Fig. 1 Electronic transport regimes around the *genuine* Mott insulator-metal transition at half filling. a Tuning the bandwidth W, for instance by chemical or physical pressure, transforms a Mott insulator to a correlated metal. Dynamical mean-field theory predicts a first-order transition with phase coexistence (delimited by solid lines) up to the critical endpoint[6], and a quantum-critical regime associated with the quantum Widom line (QWL, dashed black line) above T_{crit}[16]. The metallic state is confined by the Brinkman-Rice temperature T_{BR} (dashed cyan) at $T > T_{crit}$, the coherent Fermi-liquid regime by T_{FL} (dashed blue). When interactions U are comparable to W, and $T \gg T_{crit}$, semiconducting behavior prevails; neither a gap nor a quasiparticle peak are stabilized. **b–d** Resistivity signatures of the crossovers in dc transport. **b** The steepest slope of $\ln\{\rho(p)\}$ indicates the crossing of the QWL upon a pressure sweep. **c** T_{BR} indicates the transition from an insulating ($d\rho/dT < 0$) to a metallic ($d\rho/dT > 0$) temperature dependence. **d** The $\rho(T) \propto T^2$ behavior extends up to T_{FL}.

A more direct insight into the coexistence region was provided by spatially resolved optical spectroscopy[25]. The most compelling results came from near-field infrared experiments on VO_2 by Basov and collaborators[26] where a spatial separation of metallic and insulating regions upon heating could be visualized, in accord with X-ray studies[10,27]; the range of hysteresis in $\rho(T)$ coincides with the observed phase coexistence. Although recent developments in cryogenic near-field instrumentation are rather promising[28–30], they fall short of covering the regime $T < T_{crit} \approx 15$ K required here and do not allow for pressure tuning. For this reason, we suggest dielectric spectroscopy as a powerful bulk-sensitive method in order to unravel the coexistence regime, distinguish the individual phases and obtain a deeper understanding of the dynamics around the IMT. The complex conductivity $\sigma_1 + i\sigma_2$ not only reveals the closing of the Mott gap but yields insight into the growth of metallic regions and the formation of quasiparticles as correlation effects decrease.

Here we tackle the fundamental question whether the electrodynamic response around the Mott IMT is overwhelmed by the gradual decrease of the Mott-Hubbard gap within a homogeneous insulating phase, or whether the effects of phase coexistence dominate. Furthermore, is it possible to distinguish on the metallic side between the coherent (quasiparticle) low-T regime and incoherent transport at high-T? To answer these questions, we present temperature- and frequency-dependent dielectric measurements on a genuine Mott compound that is bandwidth-tuned across its first-order IMT. In addition to hydrostatic pressure we developed an innovative approach of chemically substituting the organic donor molecules. The experimental findings are complemented by dynamical mean-field theory (DMFT) calculations, incorporating spatial inhomogeneities in a hybrid approach. We conclude that electronic phase segregation plays a crucial role, leading to percolative phenomena due to the separation of insulating and metallic regions, also

allowing clear and precise mapping of different dynamical regimes around the IMT.

RESULTS

Mott transition through pressure and chemical substitution

We have chosen κ-(BEDT-TTF)$_2$Cu$_2$(CN)$_3$ single crystals for our investigations because this paradigmatic QSL candidate is well characterized by electric, optical and magnetic measurements[3,14,15,21,31,32]. Although the dimerized charge-transfer salt possesses a half-filled conduction band, strong electronic interaction $U \approx 250$ meV stabilizes a Mott-insulating state below the QWL ($T_{QWL} \approx 185$ K at ambient pressure[5,15]) with no magnetic order observed down to mK temperatures[3]. The effective correlation strength U/W can be reduced by increasing the bandwidth W; for pressure $p > 1.4$ kbar the metallic state is reached at low temperatures, with $T_{crit} \approx 15–20$ K. In addition, we exploited an alternative route of partially replacing the S atoms of the donor molecules by Se, where more extended orbitals lead to larger bandwidth (see sketches in Fig. 2h, k). The substitutional series κ-[(BEDT-TTF)$_{1-x}$(BEDT-STF)$_x$]$_2$Cu$_2$(CN)$_3$ ($0 \le x \le 1$, abbreviated κ-STF$_x$) spans the interval ranging from a Mott insulator to a Fermi-liquid metal. Details on the sample characterization and experimental methods are given in Supplementary Note 1. Here we focus on the out-of-plane dielectric response measured from $f = 7.5$ kHz to 5 MHz down to $T = 5$ K. Both physical pressure and BEDT-STF substitution allow us to monitor the permittivity while shifting the system across the first-order IMT.

Metal-insulator transition mapped by dielectric permittivity

Figure 2 displays the temperature-dependent conductivity and permittivity data of κ-(BEDT-TTF)$_2$Cu$_2$(CN)$_3$ when p rises (a–e) and x increases in κ-STF$_x$ (f–j). The insulating state ($p < 1.4$ kbar, $x < 0.1$), characterized by $d\sigma_1/dT > 0$, generally features small positive $\varepsilon_1 \approx 10$. The relaxor-like response previously observed in the parent compound below 50 K has been subject of debate[33,34]. The metallic state ($p > 3$ kbar, $x > 0.2$) is defined by $d\sigma_1/dT < 0$ and, concomitantly, $\varepsilon_1 < 0$ that becomes very large at low T as itinerant electrons increasingly screen. Comparison of the results in Fig. 2j with optical data measured on the same substitution yields fair agreement of the metallic values $\varepsilon_1 < 0$ (see Supplementary Fig. 7). This onset of metallic transport identifies T_{BR}[19]; while thermal fluctuations prevail at higher T, the quasiparticle bandwidth is the dominant energy scale for $T < T_{BR}$. Below T_{FL} the resistivity $\rho(T) \propto T^2$ indicates the Fermi-liquid state (see Fig. 1).

Right at the first-order IMT, however, the dielectric behavior appears rather surprising. When approaching the low-temperature phase boundary, ε_1 rapidly increases by several orders of magnitude. This colossal permittivity enhancement is more pronounced in the quasi-static limit, $\varepsilon_1 \approx 10^5$ at $f = 7.5$ kHz, and the peak value approximately follows a $f^{-1.5}$ dependence. The overall range in T and p/x of the divergency is robust and does not depend on the probing frequency (see Supplementary Figs. 4 and 8).

In Fig. 3a, b the pressure evolution of σ_1 and ε_1 is plotted for fixed T. At $T = 10$ K, $\sigma_1(p)$ rises by six orders of magnitude in the narrow range of 1 kbar. This behavior flattens to a gradual transition above 20 K, associated with the quantum-critical crossover at the QWL. The inflection point shifts to higher p, in accord with the positive slope of the phase boundary[15] associated with the rising onset of metallicity at T_{BR}. The κ-STF$_x$ series exhibits similar behavior (Fig. 3c, d): around the critical concentration of $x \approx 0.12$ a drastic increase in σ_1 is observed at low T that smears out as T rises. The maximum in $\varepsilon_1(x)$ is reached for $x = 0.16$ but broadens rapidly upon heating.
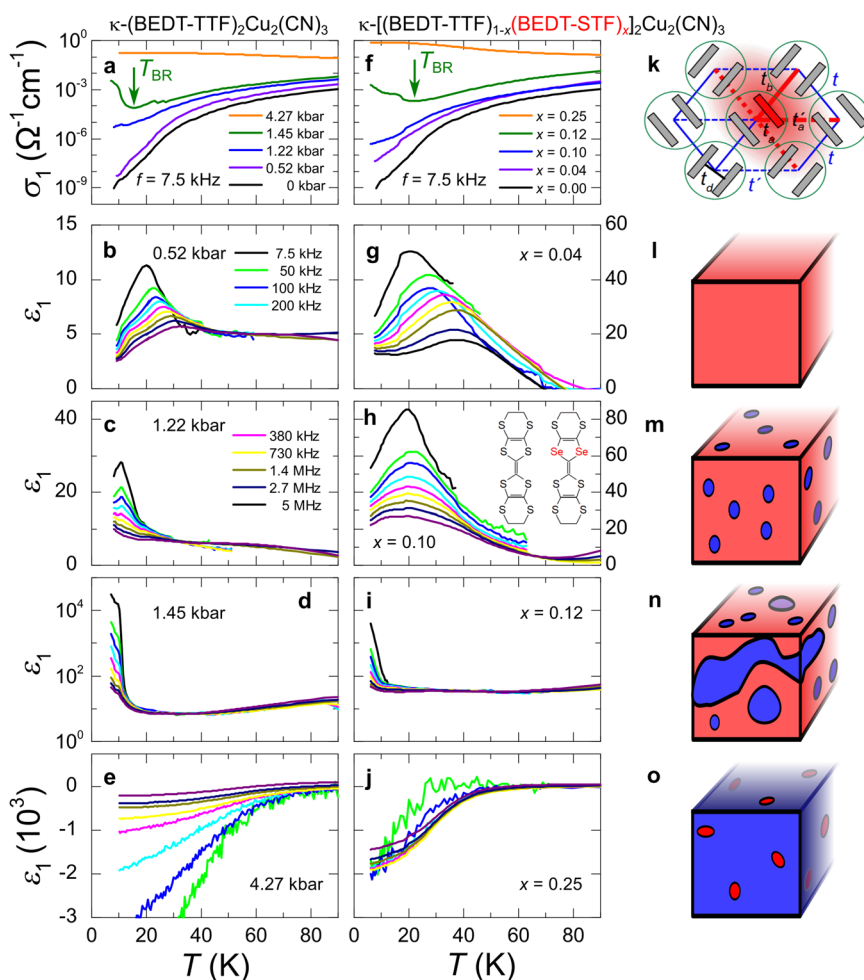
Fig. 2 Dielectric properties upon tuning through the Mott transition. The dielectric conductivity and permittivity of κ-(BEDT-TTF)$_2$Cu$_2$(CN)$_3$ were measured as a function of temperature and frequency for various applied **a–e** pressures and **f–j** chemical substitutions (introduction of Se-containing BEDT-STF molecules illustrated in **h** and **k**) that drive the system across the Mott transition. **a, f** Starting from the insulator, $\sigma_1(T)$ grows with increasing p or x; a metallic phase is stabilized below T_{BR}, in accord with dc transport[5,14,21]. **b, c, g, h** In the Mott-insulating state $\varepsilon_1(T)$ exhibits relaxor-ferroelectric behavior similar to the parent compound[33,34]. Extrinsic high-temperature contributions are subtracted. **d, i** The strong enhancement of $\varepsilon_1(T)$ at the transition is a hallmark of a percolative IMT, as sketched in **l–o**. **e, j** When screening becomes dominant in the metal, ε_1 turns negative; σ_1 exhibits Fermi-liquid behavior below T_{FL}.

Modeling phase coexistence by hybrid DMFT

The Mott IMT is based on the physical picture that a reduction of electronic correlations (i.e., the rise of W/U) gradually closes the Mott-Hubbard gap: a coherent charge response develops, causing a finite metallic conductivity. Pressure-dependent optical studies on several organic Mott insulators indeed observe this behavior[13,35]. Concerning dielectric response, it was pointed out[36] that even in the case of certain continuous IMTs, the reduction of the charge gap might induce an enhancement in ε_1, perhaps leading to a divergence at low T. Probing the optical response at THz frequencies is actually a convenient method to monitor the gap contribution to the permittivity. From p and T sweeps across the Mott IMT of several different materials, an increase by a factor of 10 is consistently reported[13,26]; in the case of κ-STF$_x$ we find it to be even smaller (see Supplementary Fig. 7). Hence, the dielectric catastrophe of $\varepsilon_1 \approx 10^5$ observed in our pressure and substitution-dependent dielectric experiments clearly signals a different mechanism at play.

To understand the physical origin of this anomaly, we recall the phase diagram of the Mott IMT at half filling, as obtained from DMFT[6,7,37,38], which has been found to successfully describe many experimental features of QSL materials[4,15] such as ours. It features a first-order IMT at low temperatures ($k_B T_{crit} \approx 0.02W$), and an

associated phase-coexistence region over an appreciable range of U/W. As in most other systems displaying phase coexistence, here we expect spatial phase segregation of the respective metallic and insulating domains, with a relative volume fraction that smoothly varies with U/W. Such a picture resembles composite materials, such as microemulsions, composites or percolating metal films[39–43]. Here we expect percolation—a phenomenon that has been long studied in a number of spatially inhomogeneous systems—to distinctly affect all physical quantities. One of the prominent consequences is a strong enhancement of ε_1 around the percolation transition, in addition to dramatic changes in the dc resistivity[44–47].

While percolation theory is by now well understood, its specific experimental manifestation may be very sensitive to the physical properties of the coexisting phases, especially in strongly correlated systems. To theoretically investigate the physical consequences of such percolative effects for our Mott system, we set up a "Hybrid DMFT" simulation across the entire phase diagram. Here we utilized DMFT to calculate $\varepsilon_1 + i\varepsilon_2$ for a single-band Hubbard model at half filling, and obtained the respective responses for both the insulating and the metallic phase as a function of T/W, U/W and frequency ω/W. Using this information on the *homogeneous* phases as input to percolation theory, we
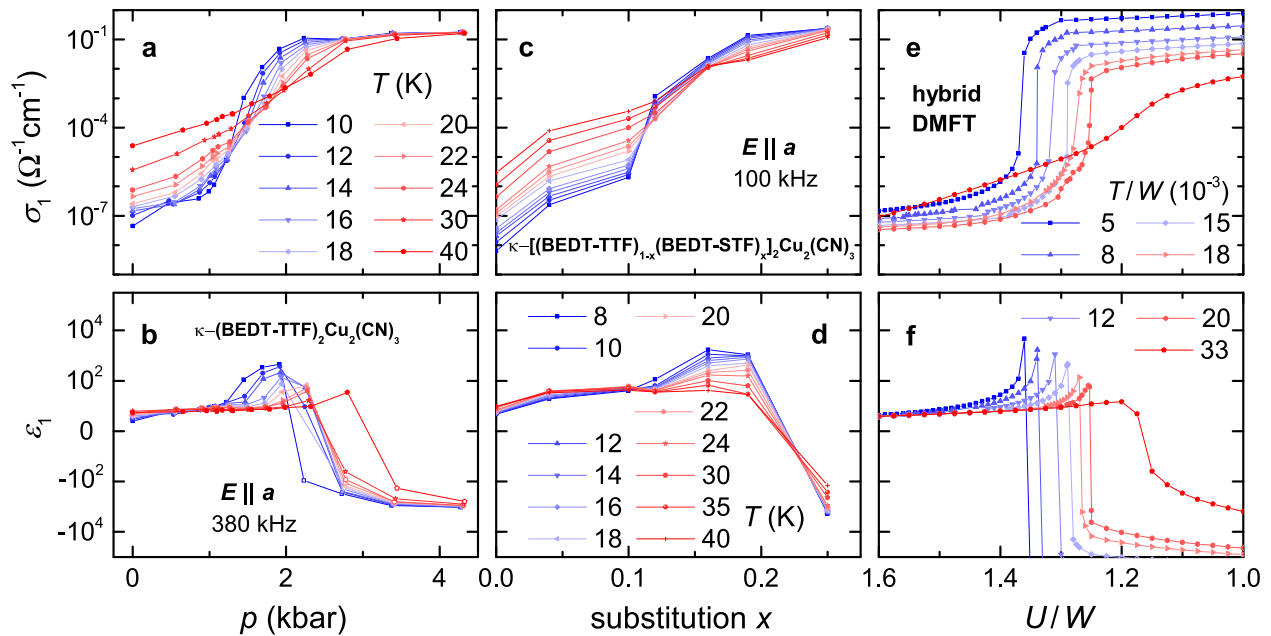
Fig. 3 Electrodynamics at the percolative Mott transition. **a** The Mott IMT of κ-(BEDT-TTF)$_2$Cu$_2$(CN)$_3$ appears as a rapid increase of $\sigma_1(p)$ that smoothens at higher T; above T_{crit} a gradual crossover remains. **b** $\varepsilon_1(p)$ exhibits a sharp peak below T_{crit}. The results at $f = 380$ kHz are plotted on a logarithmic scale. **c, d** Similar behavior is observed for chemical BEDT-STF substitution x. **e, f** Fixed-temperature line cuts of our hybrid DMFT simulations (see text) as a function of correlation strength U/W and T/W[15,16] resemble the experimental situation in minute detail, including the shift of the IMT with T. The lack of saturation of $\sigma_1(T \to 0)$ seen in DMFT modeling reflects the neglect of elastic (impurity) scattering in the metal (outside the coexistence region).

then set up an appropriate random resistor network describing the dielectric properties within the phase-coexistence region, and solved it using standard effective-medium methods[48], which suffices for our purposes.

We stress here that our Hybrid DMFT method provides a fully microscopic modeling for the physical properties of the respective phases across the phase diagram, a task that required a large-scale computational effort which we carried out in detail. In contrast, here we do not address the microscopic mechanism leading to the assumed phase separation, but instead adopt a phenomenological model (see Methods) describing how the relative volume fractions of the percolating species vary with T and U/W. In principle, spatial phase separation we envision may originate either from disorder effects[49,50], or due to inherent ("Coulomb limited") phase separation[51–53]. In either case, one expects the relative volume fraction of the respective metallic/insulating components to smoothly vary with pressure, doping or temperature, and the resulting percolative effects should be very similar. We do not expect any of the resulting anomalies to depend on the details of our phenomenological model, e.g., the strong enhancement of the dielectric permittivity or the abrupt drop of the resistivity around the percolation point (see Supplementary Note 4 for a more detailed discussion of percolation phenomena in general).

Our hybrid DMFT simulation yields excellent agreement with experiment—both pressure tuning and chemical substitution—as illustrated in Fig. 3e, f and in the false-color plots in Fig. 4. We find that the colossal peak in ε_1 is confined to the spatially inhomogeneous coexistence regime, exactly as observed in experiments. As correlation effects diminish, the dynamical conductivity (upper panels) increases from the Mott insulator to the Fermi liquid. The step in σ_1 and drop in ε_1 appear abruptly in the model but more smoothly in experiment, most likely due to inhomogeneities which broaden the coexistence regime in real materials by providing nucleation seeds for the incipient phase. Note, the percolative transition region narrows for $T \to T_{crit}$ and vanishes above that; the metallic fraction m of the simulation is

indicated in Fig. 4f. The inset of panel f clearly demonstrates that the colossal permittivity enhancement appears exclusively for a percolating mixture of metallic and insulating regions, and not for the pure phases. These results render the gap closing irrelevant for the electrodynamics at the low-temperature Mott IMT. We further point out that the discussed mechanism of a percolative enhancement of ε_1 may also apply to other related organic compounds, where similar dielectric anomalies at or nearby a first-order IMT were previously assigned to ferroelectricity[54] and multiferroicity[55].

DISCUSSION

While previous transport and optical studies[5,15] already provided hints favoring the DMFT scenario, they do not map-out the predicted dynamical regimes, especially regarding a well-defined coexistence region at $T < T_{crit}$. Our pressure- and substitution-dependent dielectric data, however, reveal all phases in vivid detail and in remarkable agreement with the respective crossover lines obtained from dc transport. Indeed, we recognize the gapped Mott insulator by essentially constant ε_1 (light red) bounded precisely by the QWL[16], while also below T_{BR}[19,20] the response clearly follows the dielectric behavior expected for a metal ($\varepsilon_1 < 0$, blue). Most remarkably, these two crossover lines converge towards T_{crit}, which marks the onset of the coexistence region, just as anticipated from Fig. 1. The emergence of phase segregation is evidenced by the huge peak of ε_1 in excellent agreement with our current DMFT-based modeling. The sharply defined boundaries of this dielectric anomaly imply that the corresponding inhomogeneities are the consequence and not the cause of phase separation, the latter resulting from strong correlation effects inherent to Mottness. Our findings substantiate that the DMFT scenario offers a rather accurate picture of the Mott IMT, in contrast to other theoretical viewpoints[56], which focus on the spin degrees of freedom in the QSL. This also confirms recent experimental and theoretical results[57,58] suggesting that such gapless spin excitations, while dominant deep within the
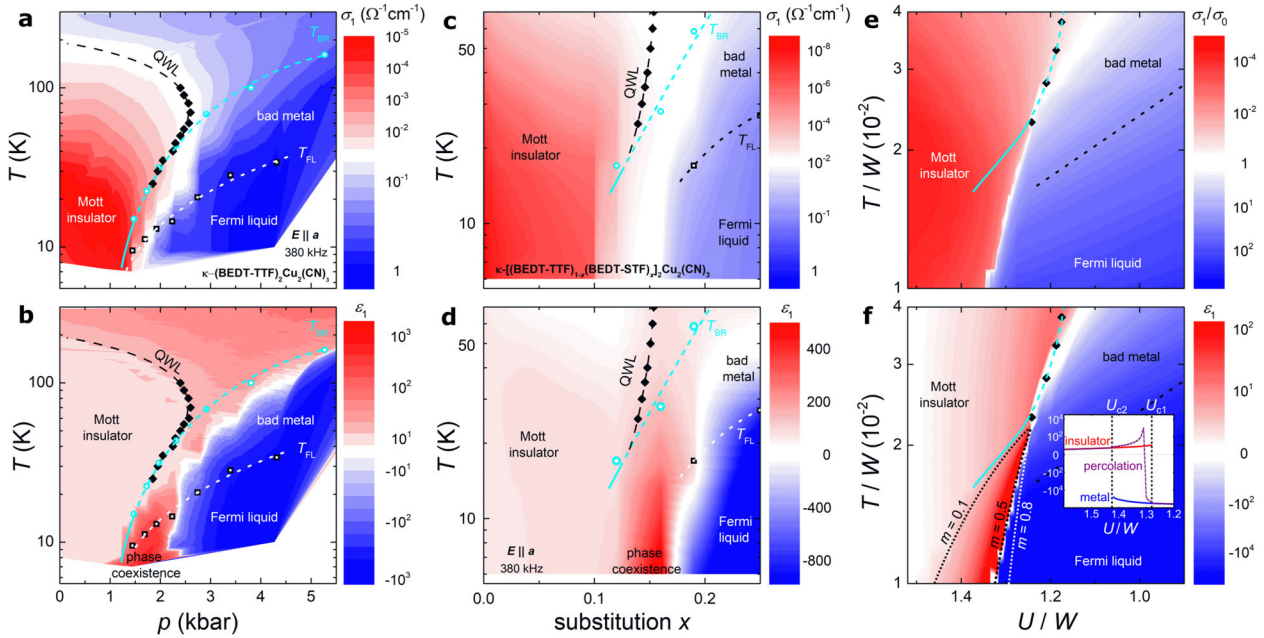
Fig. 4 Phase diagram of κ-(BEDT-TTF)$_2$Cu$_2$(CN)$_3$ when tuned through the Mott IMT. Both conductivity and permittivity exhibit similar behavior upon varying correlation strength U/W by **a**, **b** physical pressure or **c**, **d** chemical substitution, which is reproduced by **e**, **f** our hybrid DMFT calculations; the respective color codes are given to the right. In all cases, the colossal enhancement of ε_1 reveals a sharply defined insulator-metal phase-coexistence region around the first-order IMT, which is not seen in σ_1. The permittivity clearly distinguishes the Mott-insulating and metallic states via small positive and large negative values, which line up perfectly with the quantum Widom line (QWL) and the Brinkman-Rice temperature T_{BR} determined from $\sigma_1(T, p, x)$, respectively. Inset of **f**: metallic and insulating DMFT solutions are contrasted to the mixed phase (metallic fractions m indicated in main panel) that reproduces the strong peak in ε_1. Note, T_{BR} is indicated by a dashed cyan line at $T > T_{crit}$ in all panels; the resistivity maxima below T_{crit} (solid cyan line) arise due to percolative effects.

low-temperature Mott-insulating phase, are quickly damped away by the onset of charge fluctuations close to the IMT.

We demonstrated an expedient method of partial chemical substitution that triggers a similar Mott transition in κ-(BEDT-TTF)$_2$Cu$_2$(CN)$_3$ as physical pressure. The pronounced divergency in ε_1, occuring for both types of bandwidth tuning, evidences a spatial coexistence of metallic and insulating electronic phases around the first-order IMT that can be circumstantially described by DMFT blended with percolation theory. Our results yield that the Mott gap has a minor effect on the dielectric properties while the effects of phase coexistence dominate.

METHODS

Experimental

High-quality single crystals of κ-(BEDT-TTF)$_2$Cu$_2$(CN)$_3$ were grown by the standard electrochemical synthesis method[59,60] at Stuttgart and at Argonne. Plate-like single crystals of κ-[(BEDT-TTF)$_{1-x}$(BEDT-STF)$_x$]$_2$Cu$_2$(CN)$_3$ with a typical size of $1 \times 1 \times 0.3$ mm^3 were prepared according to ref.[61]; here BEDT-TTF stands for bis(ethylenedithio)tetrathiafulvalene. Substituting two of the inner sulfur atoms by selenium leads to bis-ethylenedithio-diselenium-dithiafulvalene, abbreviated BEDT-STF. Energy-dispersive X-ray spectroscopy was employed to determine the chemical composition of the alloys $0 \leq x \leq 1$[61]. The complex impedance of the crystals was measured as a function of temperature and frequency to obtain the permittivity $\hat{\varepsilon} = \varepsilon_1 + i\varepsilon_2$ and the conductivity $\hat{\sigma} = \sigma_1 + i\sigma_2$. The crystals are contacted out-of-plane ($E\|a$) by attaching thin gold wires with carbon paint to the opposite crystal surfaces. The measurements were performed with two contacts in a pseudo four-point configuration using an Agilent 4294 Impedance Analyzer. The applied ac voltage was set to 0.5 V, which was still in the Ohmic regime.

For the pressure-dependent experiments on the κ-(BEDT-TTF)$_2$Cu$_2$(CN)$_3$ crystals, we used a piston-type pressure cell ranging up to 10 kbar with a self-made electrical feedthrough for coaxial cables designed for pressure-dependent dielectric spectroscopy measurements as described in detail elsewhere[62]. Daphne oil 7373 was used as liquid pressure-transmitting medium because it is inert to molecular solids, has a good hydrostaticity

and stays fluid at room temperature for all applied pressures. The inherent pressure loss upon cooling was recorded continuously in situ by an InSb semiconductor pressure gauge[63], which shows a negligible pressure gradient below 50 K. The main temperature range discussed here is collected from the same pressure cycles; and the pressure reading at 10 K is given throughout the manuscript, unless stated otherwise. A continuous flow cryostat was utilized to cool down the pressure cell. A total cable length of only 50 cm enables measurements up to 5 MHz. The rather steep thermal gradient limits the lowest reachable temperature to 8 K, hence the superconducting state at $T \approx 4$ K[14,21] was not accessible to our dielectric experiments. No dependence on the cooling rate was observed, which was kept below 0.4 K/min for all measurements. Additional data, including analysis on the frequency dependence, can be found in Supplementary Notes 2 and 3.

Dynamical mean-field theory modeling

We performed standard[6,20] DMFT calculations of the optical conductivity σ_1 of a single-band Hubbard model at 1/2-filling, using a semicircular model density of states and iterated perturbation theory as an impurity solver, which suffices[16,17] for our purposes. The imaginary part of conductivity σ_2 was then obtained via the Kramers–Kronig transformation, and the dielectric function $\epsilon(\omega) = 1 + i\frac{4\pi}{\omega}\sigma(\omega)$ was obtained across the entire phase diagram, for both uniform phases. To describe percolative effects within the phase-coexistence region, we assumed spatial segregation of metallic and insulating regions with a smoothly varying metallic filling fraction. We used the standard effective-medium theory[64] for the corresponding random conductor/dielectric network, with a binary distribution of the local dielectric functions as calculated from DMFT for given temperature T and Coulomb repulsion U. All energies are expressed in units of the bandwidth W, i.e., T/W and U/W. For simplicity, we assign a smooth hyperbolic tangent function, as routinely used to describe phase coexistence near any first-order phase transition[49], to model the volume fraction of the metallic phase: $m(T/W, U/W) = \frac{1}{2}\tanh\{c[(T/W)_{crit} - T/W]/[(U/W)_{crit} - U/W]\} + \frac{1}{2}$, which is centered around the middle of the coexistence region: $(U/W)_{crit} = (0.20 - T/W)/0.14$. In order to match the coexistence region with the experimental data, we selected $c = 0.1$ for $U/W > (U/W)_{crit}$ and $c = 0.3$ for $U/W < (U/W)_{crit}$. More details and a visualization of the assumed metallic fraction m can be found in Supplementary Note 4.

DATA AVAILABILITY

REFERENCES
1. Shklovskii, B. I. & Efros, A. L. *Electronic properties of doped semiconductors* (Springer-Verlag, Berlin, 1984).
2. Imada, M., Fujimori, A. & Tokura, Y. Metal-insulator transitions. *Rev. Mod. Phys.* **70**, 1039–1263 (1998).
3. Kanoda, K. & Kato, R. Mott physics in organic conductors with triangular lattices. *Annu. Rev. Condens. Matter Phys.* **2**, 167–188 (2011).
4. Powell, B. J. & McKenzie, R. H. Quantum frustration in organic Mott insulators: from spin liquids to unconventional superconductors. *Rep. Prog. Phys.* **74**, 56501 (2011).
5. Furukawa, T., Miyagawa, K., Taniguchi, H., Kato, R. & Kanoda, K. Quantum criticality of Mott transition in organic materials. *Nat. Phys.* **11**, 221–224 (2015).
6. Georges, A., Kotliar, G., Krauth, W. & Rozenberg, M. J. Dynamical mean-field theory of strongly correlated fermion systems and the limit of infinite dimensions. *Rev. Mod. Phys.* **68**, 13–125 (1996).
7. Vollhardt, D. Dynamical mean-field theory for correlated electrons. *Ann. Phys. (Berl.)* **524**, 1–19 (2012).
8. Limelette, P. et al. Universality and critical behavior at the Mott transition. *Science* **302**, 89 – 92 (2003).
9. Limelette, P. et al. Mott transition and transport crossovers in the organic compound κ-(BEDT-TTF)₂Cu[N(CN)₂]Cl. *Phys. Rev. Lett.* **91**, 016401 (2003).
10. Hansmann, P. et al. Mott-Hubbard transition in V₂O₃ revisited. *Phys. Status Solidi B* **250**, 1251–1264 (2013).
11. Shimizu, Y. et al. Pressure-tuned exchange coupling of a quantum spin liquid in the molecular triangular lattice κ-(BEDT-TTF)₂Ag₂(CN)₃. *Phys. Rev. Lett.* **117**, 107203 (2016).
12. Itou, T. et al. Slow dynamics of electrons at a metal-Mott insulator boundary in an organic system with disorder. *Sci. Adv.* **3**, e1601594 (2017).
13. Li, W., Pustogow, A., Kato, R. & Dressel, M. Transition of a pristine Mott insulator to a correlated Fermi liquid: Pressure-dependent optical investigations of a quantum spin liquid. *Phys. Rev. B* **99**, 115137 (2019).
14. Furukawa, T., Kobashi, K., Kurosaki, Y., Miyagawa, K. & Kanoda, K. Quasi-continuous transition from a Fermi liquid to a spin liquid in κ-(ET)₂Cu₂(CN)₃. *Nat. Commun.* **9**, 307 (2018).
15. Pustogow, A. et al. Quantum spin liquids unveil the genuine Mott state. *Nat. Mater.* **17**, 773–777 (2018).
16. Vučičević, J., Terletska, H., Tanasković, D. & Dobrosavljević, V. Finite-temperature crossover and the quantum Widom line near the Mott transition. *Phys. Rev. B* **88**, 075143 (2013).
17. Terletska, H., Vučičević, J., Tanasković, D. & Dobrosavljević, V. Quantum critical transport near the Mott transition. *Phys. Rev. Lett.* **107**, 026401 (2011).
18. Dobrosavljević, V., Abrahams, E., Miranda, E. & Chakravarty, S. Scaling theory of two-dimensional metal-insulator transitions. *Phys. Rev. Lett.* **79**, 455–458 (1997).
19. Radonjić, M. M., Tanasković, D., Dobrosavljević, V., Haule, K. & Kotliar, G. Wigner-Mott scaling of transport near the two-dimensional metal-insulator transition. *Phys. Rev. B* **85**, 085133 (2012).
20. Deng, X. et al. How bad metals turn good: Spectroscopic signatures of resilient quasiparticles. *Phys. Rev. Lett.* **110**, 086401 (2013).
21. Kurosaki, Y., Shimizu, Y., Miyagawa, K., Kanoda, K. & Saito, G. Mott transition from a spin liquid to a Fermi liquid in the spin-frustrated organic conductor κ-(BEDT-TTF)₂Cu₂(CN)₃. *Phys. Rev. Lett.* **95**, 177001 (2005).
22. Zaanen, J., Sawatzky, G. A. & Allen, J. W. Band gaps and electronic structure of transition-metal compounds. *Phys. Rev. Lett.* **55**, 418–421 (1985).
23. Acharya, S. et al. Metal-insulator transition in copper oxides induced by apex displacements. *Phys. Rev. X* **8**, 021038 (2018).
24. Lefebvre, S. et al. Mott transition, antiferromagnetism, and unconventional superconductivity in layered organic superconductors. *Phys. Rev. Lett.* **85**, 5420–5423 (2000).
25. Sasaki, T., Yoneyama, N., Kobayashi, N., Ikemoto, Y. & Kimura, H. Imaging phase separation near the Mott boundary of the correlated organic superconductors κ-(BEDT-TTF)₂X. *Phys. Rev. Lett.* **92**, 227001 (2004).
26. Qazilbash, M. M. et al. Mott transition in VO₂ revealed by infrared spectroscopy and nano-imaging. *Science* **318**, 1750–1753 (2007).
27. Lupi, S. et al. A microscopic view on the Mott transition in chromium-doped V₂O₃. *Nat. Commun.* **1**, 105 (2010).
28. McLeod, A. S. et al. Nanotextured phase coexistence in the correlated insulator V₂O₃. *Nat. Phys.* **13**, 80–86 (2016).
29. Post, K. W. et al. Coexisting first- and second-order electronic phase transitions in a correlated oxide. *Nat. Phys.* **14**, 1056–1061 (2018).
30. Pustogow, A., McLeod, A. S., Saito, Y., Basov, D. N. & Dressel, M. Internal strain tunes electronic correlations on the nanoscale. *Sci. Adv.* **4**, eaau9123 (2018).
31. Kézsmárki, I. et al. Depressed charge gap in the triangular-lattice Mott insulator κ-(BEDT-TTF)₂Cu₂(CN)₃. *Phys. Rev. B* **74**, 201101 (2006).
32. Čulo, M. et al. Hall effect study of the κ-(BEDT-TTF)₂X family: evidence for Mott-Anderson localization. *Phys. Rev. B* **99**, 045114 (2019).
33. Abdel-Jawad, M. et al. Anomalous dielectric response in the dimer Mott insulator κ-(BEDT-TTF)₂Cu₂(CN)₃. *Phys. Rev. B* **82**, 125119 (2010).
34. Pinterić, M. et al. Anisotropic charge dynamics in the quantum spin-liquid candidate κ-(BEDT-TTF)₂Cu₂(CN)₃. *Phys. Rev. B* **90**, 195139 (2014).
35. Faltermeier, D. et al. Bandwidth-controlled Mott transition in κ-(BEDT-TTF)₂Cu[N(CN)₂]BrₓCl₁₋ₓ: optical studies of localized charge excitations. *Phys. Rev. B* **76**, 165113 (2007).
36. Aebischer, C., Baeriswyl, D. & Noack, R. M. Dielectric catastrophe at the Mott transition. *Phys. Rev. Lett.* **86**, 468–471 (2001).
37. Kotliar, G. & Vollhardt, D. Strongly correlated materials: Insights from dynamical mean-field theory. *Phys. Today* **57**, 53–59 (2004).
38. Vollhardt, D. Dynamical mean-field theory of strongly correlated electron systems. *JPS Conf. Proc.* **30**, 011001 (2020).
39. van Dijk, M. A., Casteleijn, G., Joosten, J. G. H. & Levine, Y. K. Percolation in oilcontinuous microemulsions. A dielectric study of aerosol OT/water/isooctane. *J. Chem. Phys.* **85**, 626–631 (1986).
40. Clarkson, M. T. & Smedley, S. I. Electrical conductivity and permittivity measurements near the percolation transition in a microemulsion: I. Experiment. *Phys. Rev. A* **37**, 2070–2078 (1988).
41. Pecharromán, C. & Moya, J. S. Experimental evidence of a giant capacitance in insulator-conductor composites at the percolation threshold. *Adv. Mater.* **12**, 294–297 (2000).
42. Nan, C.-W., Shen, Y. & Ma, J. Physical properties of composites near percolation. *Ann. Rev. Mater. Res.* **40**, 131–151 (2010).
43. Hövel, M., Gompf, B. & Dressel, M. Dielectric properties of ultrathin metal films around the percolation threshold. *Phys. Rev. B* **81**, 035402 (2010).
44. Dubrov, V. E., Levinshtein, M. E. & Shur, M. S. Permittivity anomaly in metal-dielectric transitions. Theory and simulation. *J. Exp. Theor. Phys.* **43**, 1050–1056 (1976).
45. Efros, A. L. & Shklovskii, B. I. Critical behaviour of conductivity and dielectric constant near the metal-non-metal transition threshold. *Phys. Status Solidi B* **76**, 475–485 (1976).
46. Bergman, D. J. & Imry, Y. Critical behavior of the complex dielectric constant near the percolation threshold of a heterogeneous material. *Phys. Rev. Lett.* **39**, 1222–1225 (1977).
47. Bergman, D. J. The dielectric constant of a composite material A problem in classical physics. *Phys. Rep.* **43**, 377–407 (1978).
48. Choy, T. C. *Effective medium theory: Principles and applications*, 2nd edn (Oxford University Press, Oxford, 2015).
49. Dagotto, E. *Nanoscale phase separation and colossal magnetoresistance: The physics of manganites and related compounds* (Springer-Verlag, New York, 2002).
50. Suárez-Villagrán, M. Y. et al. Two-dimensional disordered Mott metal-insulator transition. *Phys. Rev. B* **101**, 235112 (2020).
51. Schmalian, J. & Wolynes, P. G. Stripe glasses: self-generated randomness in a uniformly frustrated system. *Phys. Rev. Lett.* **85**, 836–839 (2000).
52. Eckstein, M., Kollar, M., Potthoff, M. & Vollhardt, D. Phase separation in the particle-hole asymmetric Hubbard model. *Phys. Rev. B* **75**, 125103 (2007).
53. Terletska, H. & Dobrosavljević, V. Fingerprints of intrinsic phase separation: magnetically doped two-dimensional electron gas. *Phys. Rev. Lett.* **106**, 186402 (2011).
54. Gati, E. et al. Evidence for electronically driven ferroelectricity in a strongly correlated dimerized BEDT-TTF molecular conductor. *Phys. Rev. Lett.* **120**, 247601 (2018).
55. Lunkenheimer, P. et al. Multiferroicity in an organic charge-transfer salt that is suggestive of electric-dipole-driven magnetism. *Nat. Mater.* **11**, 755–758 (2012).
56. Senthil, T. Theory of a continuous Mott transition in two dimensions. *Phys. Rev. B* **78**, 045109 (2008).
57. Lee, T.-H., Florens, S. & Dobrosavljević, V. Fate of spinons at the Mott point. *Phys. Rev. Lett.* **117**, 136601 (2016).
58. Pustogow, A. et al. Low-energy excitations in quantum spin liquids identified by optical spectroscopy. *Phys. Rev. Lett.* **121**, 056402 (2018).

59. Geiser, U. et al. Superconductivity at 2.8 K and 1.5 kbar in κ-(BEDT-TTF)$_2$Cu$_2$(CN)$_3$: the first organic superconductor containing a polymeric copper cyanide anion. *Inorg. Chem.* **30**, 2586–2588 (1991).

60. Komatsu, T., Matsukawa, N., Inoue, T. & Saito, G. Realization of superconductivity at ambient pressure by band-filling control in κ-(BEDT-TTF)$_2$Cu$_2$(CN)$_3$. *J. Phys. Soc. Jpn.* **65**, 1340–1354 (1996).

61. Saito, Y., Minamidate, T., Kawamoto, A., Matsunaga, N. & Nomura, K. Site-specific ^{13}C NMR study on the locally distorted triangular lattice of the organic conductor κ-(BEDT-TTF)$_2$Cu$_2$(CN)$_3$. *Phys. Rev. B* **98**, 205141 (2018).

62. Rösslhuber, R., Uykur, E. & Dressel, M. Pressure cell for radio-frequency dielectric measurements at low temperatures. *Rev. Sci. Instrum.* **89**, 054708 (2018).

63. Beyer, R. & Dressel, M. Piston pressure cell for low-temperature infrared investigations. *Rev. Sci. Instrum.* **86**, 053904 (2015).

64. Kirkpatrick, S. Percolation and conduction. *Rev. Mod. Phys.* **45**, 574–588 (1973).

AUTHOR CONTRIBUTIONS

Dielectric spectroscopic investigations were conceived by M.D. R.R. designed and performed the experiments, supported by E.U., A.B., M.W., and Y.S. Y.T. and V.D. carried out theoretical calculations. A.P. initiated and steered the collaboration of experiment and theory. A.L., R.H., Y.S., A.K., and J.A.S. prepared the crystals. A.P., M.D., and V.D. discussed the data, interpreted the results, and wrote the paper with input from all authors. A.P., R.R., and Y.T. contributed equally to this work.

COMPETING INTERESTS

The authors declare no competing interests.

ADDITIONAL INFORMATION

Supplementary information is available for this paper at https://doi.org/10.1038/s41535-020-00307-0.

Correspondence and requests for materials should be addressed to A.P., V.D. or M.D.

Reprints and permission information is available at http://www.nature.com/reprints

Publisher's note Springer Nature remains neutral with regard to jurisdictional claims in published maps and institutional affiliations.